scientific reports

Check for updates

OPEN

Covalent immobilization of *Lepidium draba* peroxidase on chitosan-coated magnetic nanoparticles and its application in glucose biosensing

Mohadeseh Sepahi-Baghan[1], Ahmad Asoodeh[1,2]✉ & Ali Riahi-Madvar[3]✉

This study aimed to improve the functionality and stability of *Lepidium draba* peroxidase (LDP) for use in glucose biosensing. Following enzyme purification, covalent binding was optimized on chitosan-coated magnetic nanoparticles (nFe_3O_4-CS). Under the optimal conditions of 0.05 g nFe_3O_4-CS, 2.5% glutaraldehyde, and an 18 h coupling duration at 25 °C, enzyme immobilization efficiency reached 30%. The formation of the immobilized enzyme (IE) was confirmed using FT-IR, XRD, and FE-SEM. Upon immobilization, the enzyme's affinity and catalytic efficiency for TMB were elevated by 1.7 and 11.0 times, respectively, in comparison to the free enzyme. The time course of stability against heat (at 50 °C) and storage stability (after 60 days at 4 °C) of the IE exhibited an increase of more than 225% and 230% as compared with the free enzyme. Moreover, the reusability of the IE was repeated up to 11 times, retaining 40% residual activity. Finally, the applicability of the IE was compared with that of the free enzyme; data showed linearity of the glucose detection range increased 10-fold compared to the free enzyme, and the assay time decreased 3 times relative to the free one. Overall, the improved stability of the immobilized LDP supports its potential use as a suitable enzyme for biomolecule detection in clinical practice and in various industrial applications.

Keywords Colorimetric biosensor, *Lepidium draba* peroxidase (LDP), Magnetic nanoparticles, Enzyme immobilization, And glutaraldehyde cross-linking

Class III peroxidases (EC 1.11.1.7) constitute a large multigene family found in plants. They are heme-containing enzymes that catalyze the oxidation of a wide range of organic and inorganic substances through the reduction of peroxides such as H_2O_2[1,2]. These enzymes are extensively used in numerous applications, such as diagnostic kits and biosensors[3,4], decolorization and degradation of dyes[5], bioremediation of phenolic compounds[6], organic synthesis[7], and cancer treatment[8].

Horseradish Peroxidase (HRP), a member of the class III plant peroxidases, is one of the most well-known and extensively used enzymes in biotechnological, industrial, environmental, and analytical applications[9–12]. Recently, Fattahian et al.[13] introduced a novel plant peroxidase gene from *Lepidium draba*, belonging to the Brassica family, and recombinantly expressed in the prokaryotic system. Using the basic local alignment search tool (BLAST), the amino acid sequence of *Lepidium draba* peroxidase (LDP) shows 93% similarity and 89% identity with HRP C1A. Moreover, due to catalytic activity and refolding yield, it is introduced as a suitable plant peroxidase for industrial applications.

One of the main applications of plant peroxidases is in biosensors and diagnostic kits[14]. Biosensors are extensively applied in medicine[15], the food industry[16], and environmental monitoring[17]. In medicine, biosensors detect biomolecules such as glucose, cholesterol, lactate, and uric acid[18,19]. Glucose is an essential metabolite for the human body, and its elevated blood glucose levels are associated with diseases including diabetes, heart attack, kidney failure, blindness, and islet cell carcinoma[20,21]. Consequently, highly sensitive and

[1]Department of Chemistry, Faculty of Science, Ferdowsi University of Mashhad, Mashhad, Iran. [2]Cellular and Molecular Research Group, Institute of Biotechnology, Ferdowsi University of Mashhad, Mashhad, Iran. [3]Department of Molecular and Cell Biology, Faculty of Basic Sciences, Kosar University of Bojnord, Bojnord, Iran. ✉email: asoodeh@um.ac.ir; riahi.ali@gmail.com

accurate glucose determination is vital for disease prevention and clinical diagnostics. Additionally, measuring glucose concentration is important in the food industry, biology, chemistry, and environmental protection[22,23]. In the medical field, numerous analytical techniques have been developed for glucose detection, such as electrochemical[24], fluorescence, and colorimetric biosensing methods[25]. Colorimetric biosensing methods are highly promising due to their selectivity, excellent sensitivity, low cost, and the ability for results to be interpreted visually based on color change. Currently, most colorimetric glucose biosensors are based on the use of glucose oxidase (GOx) and peroxidase. GOx catalyzes the oxidation of β-D-glucose in the presence of O_2 to produce gluconic acid and H_2O_2, which further oxidizes chromogenic substrate agents in the presence of peroxidase to produce colorimetric detectable signals[20]. However, the primary challenges associated with using soluble enzymes in industrial applications are their lack of reusability and their low thermal and storage stability[26]. Immobilization is one of the developed ways to overcome these problems[5]. To date, several immobilization methods have been developed, including physical adsorption, covalent linkage, encapsulation, entrapment, and cross-linking[27,28]. Among these, covalent linkage of enzymes on carriers provides stable and strong binding, thereby minimizing enzyme leaching from the carrier surface[29,30]. In this approach, selecting an appropriate carrier (characterized by properties such as being mechanically resistant, reactive groups, and surface area) is one of the most important factors[31]. The immobilization of enzymes on solid supports is a critical factor that influences the success of enzyme-based biosensors[32].

Recently, Fe_3O_4 nanoparticles (nFe_3O_4) have attracted significant interest for enzyme immobilization because of their properties, including low toxicity, large surface area, suitable physical properties, and easy recovery and reusability from the medium using external magnetic fields[33–35]. Furthermore, modification of nFe_3O_4 with biopolymers such as chitosan can protect the nanoparticles from oxidation and provide functional groups (e.g., amino, hydroxymethyl, and hydroxyl), necessary for enzyme immobilization[34,36].

Chitosan (CS), poly (1–4)-2-amino-2-deoxy-D-glucose, is a polysaccharide derived from the partial deacetylation of chitin. Due to its excellent biochemical properties, including biocompatibility, biodegradability, availability, low cost, non-toxicity, and antibacterial activity, chitosan has found widespread applications[29,37–40]. So far, numerous studies have reported the use of chitosan-iron oxide nanoparticles for enzyme immobilization within the framework of biosensor development[41–44].

In this work, glutaraldehyde-activated, chitosan-coated Fe_3O_4 nanoparticles (nFe_3O_4-CS-GDA) were used as an appropriate support for the immobilization of the recombinant LDP enzyme. Immobilization conditions, including GDA concentration, coupling time, and the amount of the support, were optimized to achieve the maximum immobilization efficiency. Subsequently, confirmation of the immobilizing enzyme on the support, physicochemical and kinetic properties, thermostability, and storage stability of the immobilized enzyme were assessed and compared with those found in the free enzyme. The reusability of the IE was evaluated, and its applicability was tested on colorimetric glucose sensing. Covalently linked LDP on the chitosan-coated Fe_3O_4 NPs (nFe_3O_4-CS) was confirmed using FT-IR, XRD, and FE-SEM. The data showed that the IE had improved affinity to the substrates (TMB and H_2O_2) and enhanced catalytic efficiency compared to the native enzyme. Furthermore, the stability of the IE against heat and storage conditions improved significantly. Finally, the applicability of the IE enzyme was tested and compared with the free enzyme in glucose sensing, with results indicating that immobilization meaningfully increased the sensitivity of the glucose detection.

Materials and methods

Materials

Ni-NTA agarose resin was purchased from Agarose Bead Technology (ABT) Company. Hemin, kanamycin, imidazole, monopotassium phosphate (KH_2PO_4), and dipotassium phosphate (K_2HPO_4) were obtained from Molekula (Gillingham, Dorset, UK). 3,3′,5,5′-tetramethylbenzidine (TMB), isopropyl-β-d-thiogalactopyranoside (IPTG), and chitosan were obtained from BioBasics (Markham, Canada). Glutaraldehyde 50% (v/v) was obtained from Zaozhuang Kerui Chemicals Co., Ltd (Shandong, China), and β-D-glucose was purchased from Merck. Glucose oxidase from *Aspergillus niger* was supplied by Sigma Aldrich. Fe_3O_4 NPs (average size of 60 nm and > 99.2 purity) were provided by NaBond Technology Inc.

LDP expression and purification

The recombinant strain (*E. coli* T7 SHuffle) containing the pET28a (+)-LDP expression system was cultured in the Luria Bertani (LB) medium according to the one-step production of soluble and active form of the peroxidase, under the Iranian patent number of 91,172. Briefly, 1 mL of overnight culture was inoculated into 100 mL of LB medium containing kanamycin (50 μg/mL) at 37 °C, 180 rpm min^{-1} until the OD_{600} reached 0.6–0.8. IPTG was then added to a final concentration of 0.1 mM, and the culture was induced at 18 °C, 180 rpm min^{-1} for 7 h. Cells were harvested by centrifugation (at 6,000×g) for 10 min. The precipitated cells were suspended in lysis buffer, sonicated for 30s, and centrifuged (at 6,000×g) for 45 min at 4 °C. The recombinant enzyme was purified through a Ni-NTA chromatography column with imidazole as an elution buffer. Purification was confirmed using 12% SDS-PAGE gel electrophoresis according to the Laemmli method[45], and the protein content was measured using the Bradford assay[46].

Determination of enzyme activity

Peroxidase activity was measured according to Krainer et al.[47]. One milliliter reaction mixture contains 10 mM H_2O_2, 0.6 mM TMB in potassium phosphate (50 mM), and 50 μL of free LDP or immobilized LDP. The change in absorbance at 653 nm (the extinction coefficient of TMB was 3.9×10^4 mol^{-1} cm^{-1}) due to TMB oxidation was recorded at 30s intervals. One unit of LDP activity was defined as the enzyme amount needed for the oxidation of 1 μmol TMB in 1 min at 25 °C and pH 6.0.

Synthesis of chitosan-coated magnetic nanoparticles

Chitosan-coated magnetic nanoparticles were synthesized as reported by Lin et al.[48], with minor modifications. In brief, 0.25 g of chitosan (CS) was dissolved in acetic acid (1%, 50 mL). Afterwards, 2 g of magnetic nanoparticles (nFe_3O_4) were added to this solution, and the mixture was stirred vigorously at room temperature. After 30 min, 50 mL of 1 M NaOH was added via syringe into the mixture to prepare nFe_3O_4 coated with chitosan (nFe_3O_4-CS). The particles were washed repeatedly with deionized water until a neutral pH was achieved and then dried at 50 °C in a vacuum oven.

Immobilization of the LDP

In the current study, LDP was covalently anchored on nFe_3O_4-CS using glutaraldehyde (GDA). To achieve optimal immobilization efficiency, several parameters including GDA concentration (1.25, 2.5, and 5% (v/v)), coupling durations (2, 4, 6, 18, and 20 h), and the quantity of support (0.2, 0.1, and 0.05 g), were evaluated in presence of constant enzyme concentration (1 mg/mL) in the immobilization mixture. Then after, the resulting nanostructures were washed 3 times with deionized water to remove excess unbounded components such as glutaraldehyde. Subsequently, 6 mL of 1 mg/mL LDP solution was added to GDA GDA-activated support. After gentle stirring at 25 °C for 18 h, the product was collected magnetically using an external magnet, before being washed three times with phosphate buffer (50 mM, pH 7.0), and then collected. The resulting nFe_3O_4-CS-GDA-LDP was resuspended in 2 mL of PBS buffer (50 mM, pH 7) for further use.

The LDP immobilization efficiency was calculated according to Eq. (1)[36]:

$$\text{Immobilization efficiency } [\%] = \frac{\text{The concentration of protein immobilized on the } nFe_3O_4 - CS \text{ carrier}}{\text{Total protein concentration of free LDP}} \times 100 \quad (1)$$

The concentration of protein immobilized on the nFe_3O_4–CS carrier was calculated as the total protein concentration minus the concentration of unbound protein in the supernatant.

Characterization of nFe_3O_4-CS-GDA-LDP

Immobilization of the enzyme on the nanostructure was confirmed using techniques such as FTIR, XRD, FE-SEM, and EDX analyses.

FTIR spectra of nFe_3O_4, nFe_3O_4-CS, and nFe_3O_4-CS-GDA-LDP were recorded in the range of 4000–400 cm^{-1} by Thermo Nicolet AVATAR 370 (Courtaboeuf, France). X-ray diffraction (XRD) measurements: crystal structure of the samples was obtained using a XRD Rigaku Ultima IV in the laboratory of the Mahamax, an online characterization platform in Tehran, Iran. FE-SEM images of the samples were studied using MIRA3 LMU (Tescan Company, Czech Republic). The chemical composition analysis was performed using the energy-dispersive X-ray spectroscopy (EDX).

Optimum pH and temperature

To measure optimum pH, the residual activities of both free and IE were evaluated at different pH values at room temperature (25 °C). The buffers used were sodium acetate (pH 3.0–5.6, 50 mM) and potassium phosphate (pH 5.8-8.0, 50 mM)[49]. To obtain the optimum temperature, residual activities of the free and the IE were investigated in potassium phosphate buffer (50 mM) under the optimum pH with temperatures ranging from 15 °C to 40 °C. The results were presented as residual activity based on the amount of protein present in the free and immobilized samples.

Thermal stability and half-life of the free and the immobilized LDP

Thermostability was measured by incubating free and immobilized LDP at different temperatures (20–50 °C) for 10 min. Following incubation, samples were kept in an ice bath for 5 min, and enzyme activity was measured as described in "Determination of enzyme activity" section.

Deactivation rate constant (k_d) was determined from the Arrhenius plot of log residual activity (%) in relation to time (min) using Eq. (2)[50]:

$$\text{Slope} = k_d \quad (2)$$

The half-life ($t_{1/2}$) of the enzymes, determined as the duration required for the enzyme to diminish to 50% of its initial activity[51], was calculated using Eq. (3):

$$t_{1/2} = Ln\ 2/k_d \quad (3)$$

wherein $t_{1/2}$ (min) represents the half-life of the enzyme and k_d (min^{-1}) denotes the thermal inactivation rate constant.

Kinetic parameters

The kinetic parameters, Michaelis-Menten constant (K_m) and maximum reaction velocity (V_{max}) of the free and the immobilized LDP were determined using different substrate concentrations of TMB and H_2O_2. The constant concentration of TMB (0.6 mM) was examined with various concentrations of H_2O_2 (0.01 to 20 mM) in optimum conditions. Furthermore, various concentrations of TMB (0.01 to 1 mM) were evaluated in the presence of a constant concentration of H_2O_2 at 10 mM. The turnover number (k_{cat} s^{-1}) for both the free and IE was determined using Eq. (4):

$$k_{cat} = V_{max}/E_T \tag{4}$$

In this context, V_{max} (mM.s^{-1}) represents the maximum reaction velocity, while [E_T] pertains to the total concentration (mM) of enzymes present within the reaction medium. The catalytic efficiency constant (s^{-1}·mM^{-1}) for both free and immobilized LDP was derived as the turnover number (k_{cat} s^{-1}), and the Michaelis-Menten constant, as delineated in Eq. (5):

$$\text{Catalytic efficiency} = k_{cat}/k_m \tag{5}$$

Storage stability of the free and immobilized LDP

Storage stability of the free and immobilized LDP was assessed by quantifying their residual enzymatic activities over 60 days at 4 °C in a phosphate buffer solution (pH 6.0, 50 mM). Residual enzymatic activities were quantified at designated intervals (every 7 days) employing the following equation [51]:

$$\text{Residual activity}\,(\%) = (E/E_0)\,100 \tag{6}$$

where E and E_0 denote the enzymatic activities at time t (min) and at the initial time point, t = 0 min, respectively. The initial activity of the free and IE was considered 100%.

Reusability of the immobilized LDP

To assess the reusability of the immobilized LDP, a singular reaction cycle was conducted in a volume of 1.0 mL of reaction mixture, which comprised 10 mM H_2O_2, 0.6 mM TMB, and a 50 mM phosphate buffer (pH 6.0). Subsequently, the immobilized LDP was washed three times with phosphate buffer at pH 6.0, using an external magnet to eliminate any residual substrate, and then reintroduced into the subsequent reaction cycle. The residual activity after each cycle was determined as described in "Storage stability of the free and immobilized LDP" section.

Glucose detection concentration

Glucose detection was carried out as follows: 25 µL GOx (1 mg/mL), different concentrations of glucose (0.1, 0.2, 0.4, 0.8, 1, 3, 5, and 10 mM), and 50 mM phosphate buffer (pH 6.0) were mixed in a final volume of 500 µL and incubated at 37 °C for 45 min. Then LDP enzyme (free or immobilized) (0.3 mg/mL), TMB (0.6 mM), and 50 mM phosphate buffer (pH 6.0) were added. After 10 and 30 min incubation at 37 °C, the color intensity of the mixtures was measured at 653 nm using UV-spectroscopy (Termo Scientific Evolution 300). The limit of detection value was calculated using Eq. (7)[52]:

$$\text{LOD} = \frac{3\ \text{Standard deviation of blank}}{\text{Slop of calibration curve}} \tag{7}$$

Results and discussion

Expression and purification of the Recombinant LDP

LDP expression was carried out using the T7 SHuffle strain in the presence of 0.1 mM IPTG, and the subsequent purification process was achieved using a Ni-NTA-Sepharose affinity chromatography column. The purified proteins were analyzed on 12% SDS-PAGE, and the recombinant LDP was estimated to be approximately 34 KD of a single band as deduced from SDS-PAGE (Fig. 1). The high quality of the purified protein (> 95%) was observed in lanes 3, 4, 5, 6, and 7. These fractions were collected and stored at -20 °C to be applied for further studies.

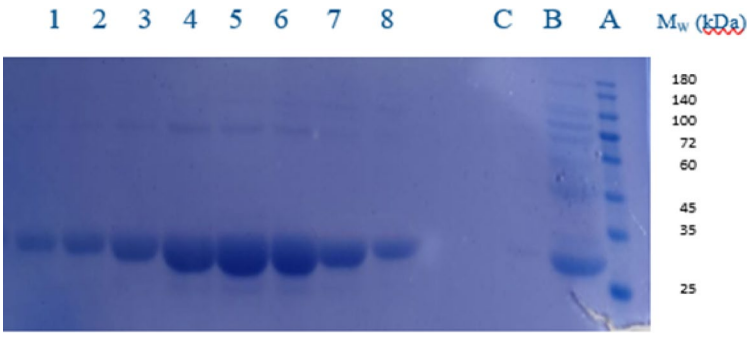

Fig. 1. SDS-PAGE of the purified recombinant LDP with different concentrations of imidazole, lane "A" is the protein ladder, lane "B" is the before column sample as control, lane "C" is the eluted sample passed from the column with wash buffer, Lane umbers 1, 2, 3, 4, 5, 6, 7, and 8 are related to the protein output from the column with concentrations of 300, 300, 250, 250, 200, 200, 100, 50 mM imidazole, respectively.

Immobilization efficiency

To obtain the highest residual activity and immobilization efficiency of the IE, several factors, including GDA concentration, coupling time, and the amount of support, were tested in phosphate buffer (50 mM, pH 6.0) containing a constant enzyme concentration of 1 mg/mL at 25 °C. Among the tested support concentrations, only 0.05 g yielded results (data not shown). The effect of GDA concentration on the remaining activity and immobilization efficiency of the enzyme is shown in Fig. 2a. As revealed in the figure, the lowest and highest GDA concentrations yielded lower residual activity of the IE than was observed at 2.5% GDA concentration. This can be attributed to the inadequacy of low GDA concentrations to generate sufficient crosslinking for the enzyme; conversely, an excessive crosslinking may lead to a distortion of the enzyme's tertiary structure[53]. Such structural distortion may impede the accessibility and accommodation of the substrate, consequently affecting the retention of enzyme activity[54]. Therefore, 2.5% was chosen as the optimal GDA concentration for enzyme immobilization; under these conditions, the highest immobilization efficiency was obtained (30%).

In Fig. 2b, the impact of coupling time on residual activity and immobilization efficiency is depicted. As shown in the figure, the residual activity of the IE was gradually elevated by increasing immobilization time, so that the maximum was observed at 18 h, and by increasing coupling time over 18 h, residual activity changed considerably. This may occur because the immobilization of the enzyme on the support reached a saturated duration of 18 h. With the extension of the reaction time, any augmentation in the quantity of IE may significantly enhance the steric hindrance experienced by the IE molecules, resulting in a slight reduction in enzyme activity. By increasing the immobilization time, immobilization efficiency was also improved, so that it reached a maximum of 30% after 18 h.

According to the results, under the experimental conditions in phosphate buffer (50 mM, pH 6.0) containing 0.05 g of nFe_3O_4-CS, 1.0 mg/mL of LDP, and at 25 °C, the optimal GDA concentration and incubation time were obtained at 2.5% (v/v) and 18 h, respectively. Similar results regarding the GDA concentration and coupling time were reported by several studies which were conducted to immobilize HRP on a nanostructure by the use of GDA. For example, Lu et al.[55] documented the immobilization of HRP on glutaraldehyde-activated carbon nanospheres using 2% glutaraldehyde (GDA) (v/v), with a coupling time of 18 h at 25 °C. Zai et al.[56] successfully immobilized HRP on chitosan–halloysite hybrid-nanotubes (CTS–HNT) using 2.5% GDA, at 4 °C for 15 h. Keshta et al.[27] documented immobilization of HRP on Fe_3O_4@NH_2 NPs at room temperature overnight.

Under optimal immobilization conditions, an immobilization efficiency of 30% was obtained. El-Shishtawy et al.[51] immobilized the catalase enzyme on chitosan-coated zinc oxide nanoparticles. They reported an immobilization efficiency of 37%. Jankowska et al.[57] reported a 27% immobilization yield for the covalent immobilization of HRP on Electrospun fibers. Gomez et al.[58], using glutaraldehyde as a coupling agent to immobilize HRP on glass beads, reported a 40% immobilization efficiency. Chagas et al.[59] showed that the immobilization efficacy of turnip peroxidase on chitosan beads was 51%.

Immobilized confirmation

FT-IR spectra analysis

The FT-IR spectra of naked nFe_3O_4, nFe_3O_4-CS, and nFe_3O_4-CS-GDA-LDP are shown in Fig. 3. For naked nFe_3O_4, an absorption band at approximately 598 cm^{-1} corresponds to the Fe-O stretching vibrations (Fig. 3a)[60]. In nFe_3O_4–CS NPs (Fig. 3b), the band at 1073 cm^{-1} is attributed to C-O-C stretching vibrations, demonstrating the binding of chitosan to the nFe_3O_4 NPs[61]. In Fig. 3c, the band at about 1061 cm^{-1} (C–N bond) shows the crosslinking of GDA to chitosan[62]. Furthermore, new bands observed at around 1651 cm^{-1} and 1541 cm^{-1}

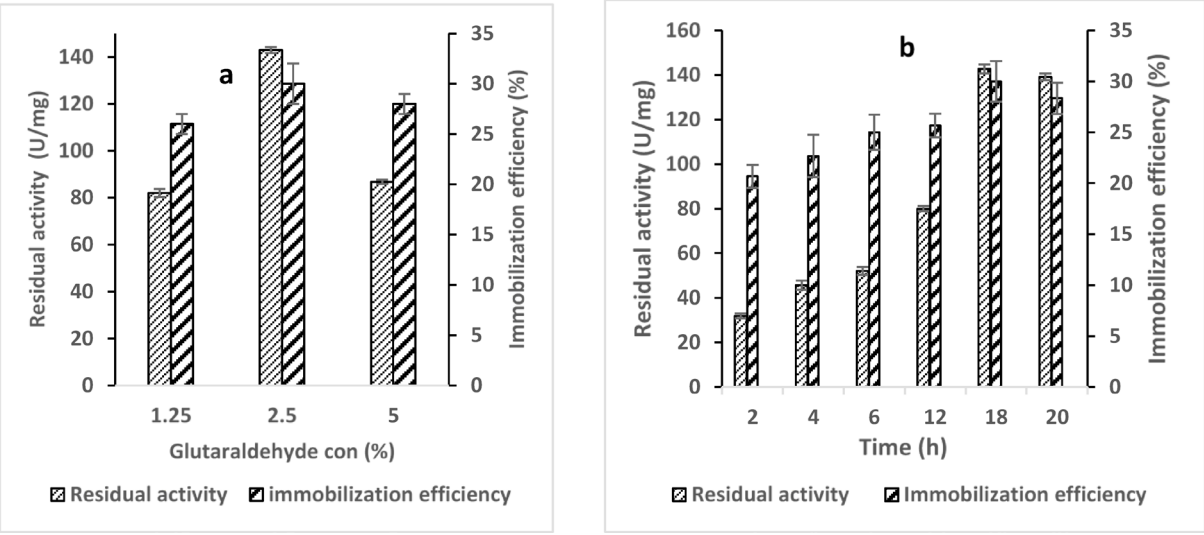

Fig. 2. (**a**) Optimization of glutaraldehyde concentrations and (**b**) time of coupling for LDP immobilization on the support.

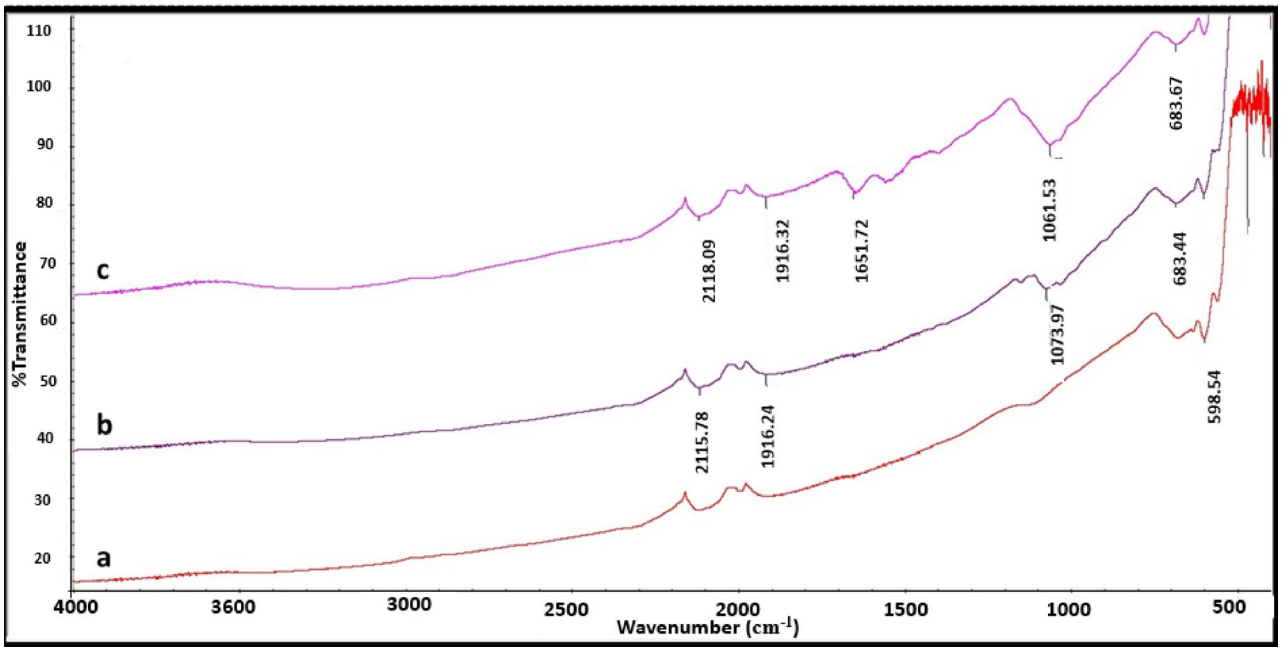

Fig. 3. FT-IR spectra of (**a**) nFe_3O_4, (**b**) nFe_3O_4-CS, and (**c**) immobilized LDP.

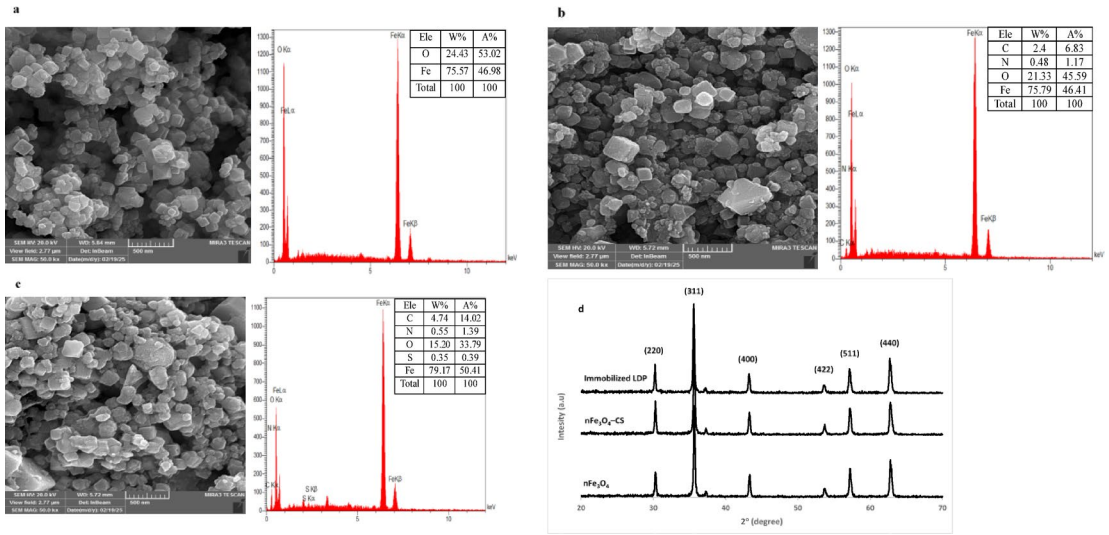

Fig. 4. FE-SEM images and corresponding EDX spectra of (**a**) nFe_3O_4, (**b**) nFe_3O_4-CS, and (**c**) immobilized LDP. E: Elements; W: Weight; A: Atomic. XRD pattern of the samples (**d**).

correspond to the –CONH– (amide I) and amide II vibrations of protein[34,63], confirming the binding of the enzyme to the support.

FE-SEM analysis

FE-SEM images (Fig. 4a–c) provide a detailed examination of nFe_3O_4, nFe_3O_4-CS, and immobilized LDP. The surface morphology of the chitosan-coated and immobilized nanoparticles exhibited significant changes: nanoparticle surface roughness increased following chitosan treatment, subsequent glutaraldehyde activation, and enzyme immobilization. The coating of the surface with chitosan and the enzyme's subsequent attachment to the activated surface could be the cause of this phenomenon[64]. Additionally, the EDX spectrum of Fe_3O_4 showed the presence of iron and oxygen, and the Fe_3O_4-CS spectrum revealed the presence of carbon, nitrogen, iron, and oxygen. Finally, the EDX spectrum of the immobilized LDP showed the presence of carbon, nitrogen, iron, oxygen, and sulfur. Therefore, the EDX results confirmed the presence of the essential elements in the respective materials, as shown in Fig. 4a a–c, which confirmed the immobilization of the enzyme on the support.

XRD analysis

Figure 4d illustrates the XRD patterns corresponding to the naked nFe_3O_4, nFe_3O_4-CS, and immobilized LDP, wherein six distinctive peaks associated with nFe_3O_4 were identified (220, 311, 400, 422, 511, and 440) across all samples. The identified peaks show that the synthesized nanoparticles are comprised of pure nFe_3O_4 exhibiting a spinel crystallographic structure. These results suggest the nanoparticles preserved the crystalline structure of nFe_3O_4 after the chitosan coating and enzyme immobilization processes[34,38].

Effect of pH and temperature on the free and immobilized LDP activity

The effect of pH on the activity of immobilized LDP and free LDP was studied in the pH range of 3.0–8.0 at 25 °C (Fig. 5a). Both enzyme forms exhibited maximum activity at pH 6.0, which was considered the optimal pH value. This finding is consistent with the findings documented for most plant peroxidases, which typically show optimal enzymatic activity in the pH range of 4.5 to 6.0[27]. In Patel et al.[65], the optimal pH values for HRP activity were determined to be 6 and 7 on rGO-Fe_3O_4-M1 and Fe_3O_4 particles, respectively. Chang et al.[66] reported that immobilization of HRP on a superparamagnetic Fe_3O_4/graphene oxide nanocomposite yielded similar optimal pH values of approximately 6.4 for both free and immobilized HRP. In another study, Muley et al.[67] explained that the immobilization of cellulase on iron oxide magnetic nanoparticles did not change the optimal pH, which remained between 6.0 and 6.5. Compared to the free LDP, the immobilized LDP exhibited higher residual activity across all pH values, indicating improved pH adaptability. This phenomenon may be attributed to the covalent interactions between the enzyme and chitosan-coated magnetic nanoparticles (CMNP), which have potentially constrained the conformational changes, resulting in enhanced stability across an extended pH spectrum[68]. It should be noted that the IE exhibited the highest residual activity from pH 3 to 7, while for free LDP peak activity was from pH 5 to 7.

The optimum temperature of the free and immobilized LDP was determined by measuring residual activity across a temperature range from 15 °C to 40 °C at optimal pH, as is shown in Fig. 5b. The optimum temperature of the free LDP was recorded at 30 °C, while the immobilized LDP peaked at 25 °C (room temperature). In widely circulated literature, it was documented that the optimum temperature of the IEs shifts towards higher[29,49,69] or lower[70–72] values compared to the related free enzymes. The high residual activity of the immobilized LDP at room temperature facilitates its application in diagnostic kits. Compared to the free LDP, the immobilized LDP demonstrated higher residual activity, demonstrating that immobilized LDP had better activity at a temperature range from 20 to 40 °C. Chattopadhyay & Mazumdar observed that HRP exhibited its highest activity at temperatures of 25–40 °C[11]. Moreover, Xie et al.[73] reported that, compared with free HRP, the stability and enzymatic activity of the immobilized HRP on Fe_3O_4@PAA-6-armPEG-NH_2 showed a significant enhancement across a broad temperature range. Generally, interactions between enzymes and between the enzyme and its

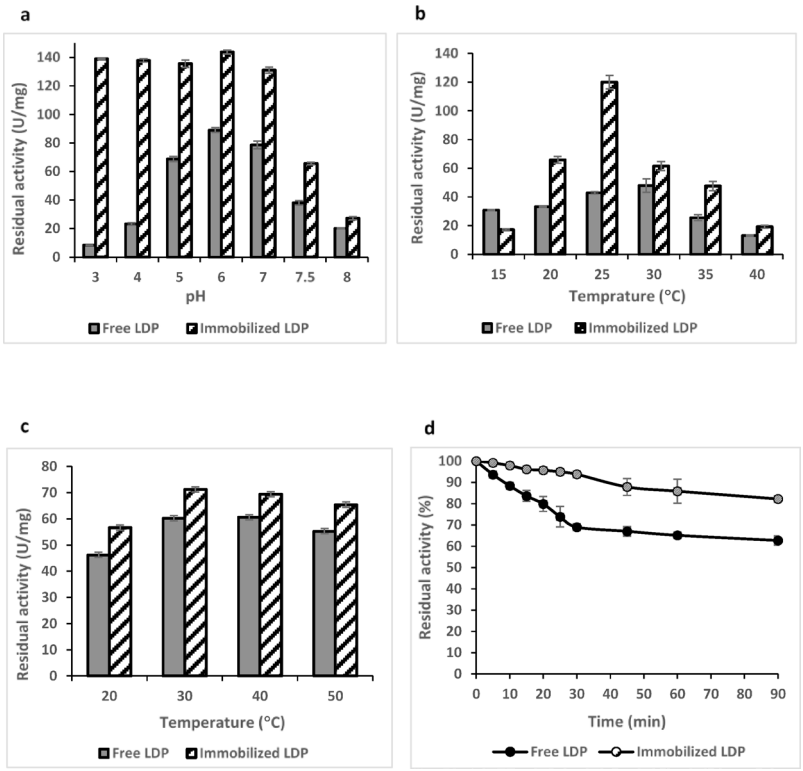

Fig. 5. Effect of (**a**) pH and (**b**) temperature on residual activity of the free and immobilized LDP. (**c**) Thermal stability of LDP enzyme. (**d**) Time course of stability against heat of the free and immobilized LDP at 50 °C. Bars show one standard deviation of the mean (n = three replicates).

support increase with increasing temperature, which may affect the enzyme's optimal temperature[74]. However, immobilization of LDP on the Zn-MOF nanostructure[70] and surface mutation (N186R and N198R)[75] has been reported to decrease the optimum temperature, and this decrease was accompanied by changes in the enzyme structure. Consequently, it may be speculated that the LDP structure was also affected through covalent immobilization on CS-nFe_3O_4.

Thermal stability and half-life of the free and immobilized LDP

Thermal stability of the free and immobilized LDP was studied at various temperatures ranging from 20 to 50 °C. As shown in Fig. 5c, IE exhibited better thermal stability across all temperatures, approximately 10% higher stability compared to the free one. On the other hand, the free and immobilized LDP displayed maximum activity at temperatures ranging from 30 to 40 °C, a similar pattern that was reported recently by Farhadi et al.[70]. Furthermore, Huang et al.[76] reported that the lipase, which was covalently immobilized on magnetic iron nanoparticles by the carbodiimide, showed enhanced stability in response to variations in temperature.

The time courses of enzyme stability against heat during a 90 min test at 50 °C are shown in Fig. 5d. The residual activity of the free and immobilized LDP was 62.67% and 82.18%, respectively. After 30 min incubation of the enzymes at 50 °C, approximately 7% of the initial activity was lost for IE and more than 30% for the free enzyme. The deactivation rate constant (k_d) is an important parameter for advancing economic bioprocesses at an industrial scale[30]. At 50 °C, the k_d for the IE was 0.0023 min^{-1}, which is lower than that of the free enzyme (0.0052 min^{-1}). A lower k_d for the immobilized LDP signifies a lower rate of denaturation[77]. Additionally, the half-life ($t_{1/2}$) of the enzyme at this temperature increased from 133.30 min (for the free enzyme) to 301.37 min upon immobilization, suggesting that immobilization of the enzyme effectively enhances its thermostability. To date, literature has reported that stability and resistance to temperature variation improve upon enzyme immobilization[78]. Covalent immobilization of an enzyme to a support often limits its conformation, thereby leading to greater resilience against thermal denaturation[79].

Kinetic parameters

As summarized in Table 1, K_m values of the immobilized LDP for substrates (TMB and H_2O_2) decreased, rather than the free LDP. On the other hand, the results demonstrated that the affinity toward TMB and H_2O_2 of the immobilized LDP was drastically enhanced by a factor of 1.7 and 3.8-fold in comparison with the free counterpart. These findings are consistent with some recently reported data. For example, Farhadi et al.[70] elucidated that the immobilization of LDP on the Zn-MOF enhances enzyme affinity towards TMB by a factor of around 1.5. Gao et al.[80] reported immobilization of HRP on hierarchically porous magnetic metal-organic frameworks (HP-Zr-MOF@Fe_3O_4) also increased enzyme affinity towards the substrate by over 2.2 times.

In addition, the V_{max} of the immobilized LDP was markedly higher than that observed for the free enzyme. In particular, the V_{max} of the immobilized LDP increased by about 2 and 4-fold for TMB and H_2O_2, respectively, compared to that of the free enzyme. This enhancement may be attributed to the fact that immobilization alters the structural conformation of the enzyme and optimizes the functionality of its catalytic active site, thus facilitating an increase in the reaction rate and promoting the conversion of the substrate to product[6].

Besides, the K_{cat} and k_{cat}/K_m for immobilized LDP were higher than those for free LDP. The turnover number (k_{cat}) exhibits a significant magnitude, and the process of product formation within catalysis becomes increasingly advantageous. Furthermore, an elevated catalytic efficiency (k_{cat}/K_m) indicates a superior proficiency of the enzyme and facilitates its conversion into products (Table 1)[81]. Jaiswal et al.[82] documented that the catalytic efficiency of the immobilized laccase in chitosan beads increased more than 10-fold in comparison to that of the free form. Also, Vineh et al.[83] reported that, following the immobilization of HRP on functionalized reduced graphene oxide by covalent bonding, the k_{cat}/K_m demonstrated an approximate 8.5-fold increase. The pronounced affinity exhibited towards the substrate, coupled with the catalytic efficacy of LDP immobilized on nFe_3O_4-CS-GDA, underscores the proficiency and effectiveness of the employed support and immobilization methodology[84].

Storage stability of the free and immobilized LDP

To assess enzyme storage stability, the residual enzymatic activity was evaluated following the storage for 60 days at 4 °C. The results showed that about 20% and 46% of the initial activity of free and IE was restored after around 2 months, respectively. According to Fig. 6a, **50**% of the initial activity for the free and immobilized LDP was reduced after 23 and 48 days, respectively. These results demonstrate that enzyme immobilization improved its storage stability approximately 2-fold compared to the free enzyme. This can be due to the covalent interactions between the enzyme and the support, as reported by Sahu et al.[29]. They documented that the storage stability of the immobilized HRP on chitosan-Fe_2O_3 nanoparticle coated with graphene oxide significantly improved following covalent bonding of the HRP to the support matrix.

Enzyme form	K_m (mM)		V_{max} ($U.mg^{-1}$)		k_{cat} (s^{-1})		k_{cat}/k_m ($s^{-1}.mM^{-1}$)	
	TMB	H_2O_2	TMB	H_2O_2	TMB	H_2O_2	TMB	H_2O_2
LDP	0.051	5.5	46.30	107.53	631.14	1111.22	12393.38	201.05
Immobilized LDP	0.029	1.43	96.15	476.20	3938.83	15019.0	136546.18	10513.3

Table 1. Kinetic parameters of the free and immobilized LDP for TMB and H_2O_2.

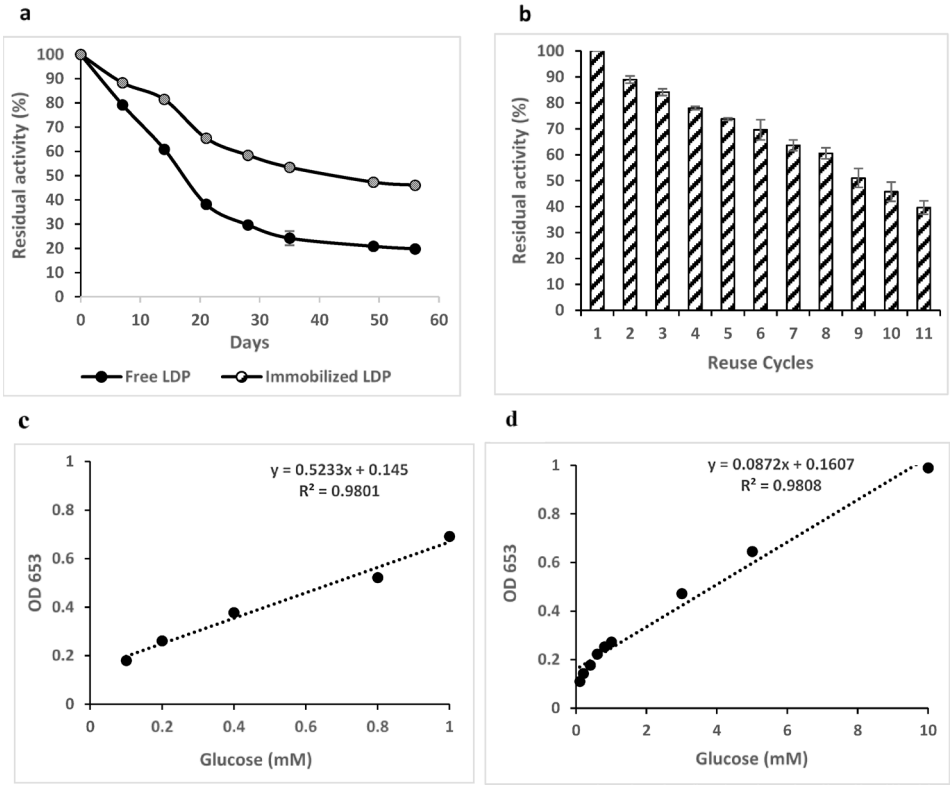

Fig. 6. (**a**) Storage stability of the free and immobilized LDP at 4 °C in the period time of 60 days. (**b**) Reusability of immobilized LDP. Bars show one standard deviation of the mean (n = three replicates). For more details, see the Experimental procedures. Spectrophotometric plot for standard glucose assay with (**c**) free LDP and (**d**) immobilized LDP.

Reusability of the immobilized LDP

Because chitosan-coated magnetic nanoparticles possess magnetic properties and biocompatibility, immobilized enzymes can facilitate recovery processes for subsequent reutilization[85].

The capacity for enzyme reusability constitutes one of the primary advantages associated with the immobilization of the enzymes. This attribute of permitting enzymes to be utilized across multiple cycles represents the most critical determinant for environmental and industrial applications, owing to its economic efficiency[29,84,86]. The performance of immobilized LDP across multiple reaction cycles is illustrated in Fig. 6b. The immobilized LDP exhibited a retention of about 73% activity over five cycles of TMB oxidation, facilitated by its rapid and efficient separation through magnetic means, indicating good operational stability of the immobilized LDP. Keshta et al.[27] reported that the HRP immobilized on Fe_3O_4@NH_2 with guaiacol as substrate retained 60% of its initial activity after 5 cycles. Mohammadi et al.[87] reported a reuse of immobilized enzyme on epoxy-functionalized silica, and showed 61% retention of its enzymatic activity subsequent to 5 cycles of use. The activities of the IE exhibited a gradual decline concomitant with an increase in the number of reuse cycles. These findings may be explained by the inactivation of the enzyme, which is attributed to the phenomena of leakage and denaturation of the enzyme. Also, the decrease may be due to the loss of particle fraction during use and washing as reported by Abdella et al. [50]. The capacity for reusability of the IE constitutes a critical determinant for practical applications aimed at minimizing expenses and simplifying procedures[36,88]. Recently, Farhadi et al.[70] reported that the process of centrifugation employed during the application of MOFs for enzyme immobilization results in the agglomeration of materials, which consequently leads to enzyme leakage, thereby adversely impacting their reusability[80]. In our work, the use of chitosan-coated magnetic nanoparticles effectively addresses this challenge by facilitating the swift separation of immobilized enzymes from the reaction medium when subjected to an external magnetic field.

Glucose detection

Glucose determination was performed based on the combined reaction of GOx and peroxidase (LDP/nFe_3O_4-CS-GDA-LDP) activity. In this process, glucose was oxidized in the presence of GOx enzyme to produce gluconic acid and hydrogen peroxide. Then, hydrogen peroxide was detected quantitatively in a colorimetric reaction of TMB to produce blue-colored oxidized TMB (ox-TMB), with a characteristic absorption peak at 653 nm[89]. The produced dye intensity represented the glucose content of the sample. As shown in Fig. 6c, d, in the presence of free LDP and immobilized LDP, the ox-TMB intensities increase with increasing concentrations of glucose in the media. The glucose biosensing process shows linearity as 0.1 to 1 mM (after 30 min) and 0.1 to 10 mM (after

Enzyme/Immobilized enzyme	Detection range (mM)	LOD (mM)	Ref.
Chitosan/polyvinyl alcohol nanofibers, GOx-HRP	2.7–13.8	2.7	[3]
Tree shape paper strip, GOx-HRP	1–11	0.3	[21]
Paper strip, GOx	0.5–75	1.23	[91]
Paper Based Device (μPAD), GOx-HRP	0.5–2.84	0.28	[92]
Chitosan film, GOx, HRP	0.1–0.8	0.033	[90]
GOx-LDP	0.1-1	0.027	This work
Fe_3O_4- CS, GOx-LDP	0.1–10	0.025	This work

Table 2. Comparison of analytical performance of some enzyme-based glucose biosensors.

10 min) for glucose solution, and a limit of detection around 0.027 and 0.025, for the free LDP and immobilized LDP, respectively. In Table 2, a comparison of the results obtained in this study and other studies on glucose colorimetric biosensors is presented. Filiz et al. [3] documented the synthesis of electrospun blended chitosan-poly (vinyl alcohol) nanofibers for a colorimetric glucose biosensor of GOx/HRP. The experimental findings showed that the colorimetric reaction was linear for glucose detection, ranging from 2.7 to 13.8 mM, with a limit of detection at 2.7 mM. Zhu et al.[21] designed a semi-quantitative approach for the determination of glucose utilizing self-calibration based on GOD/HRP bi-enzyme colorimetry through the application of tree-shaped paper strips. The linear detection range was from 1.0 to 11.0 mM, accompanied by a detection limit of 0.3 mM. Furthermore, Skonta et al.[90] presented a colorimetric glucose biosensor based on chitosan films. The linear range was observed from 0.1 to 0.8 mM with a detection limit of 0.033 mM.

Also, Soni & Jha.[91] developed a non-invasive glucose biosensor utilizing a paper strip for the analysis of saliva. The designed optical biosensor exhibited a detection range spanning from 9 to 1350 mg/dL of glucose, alongside a notable limit of detection of 22.2 mg/dL. Zhang et al.[92] constructed a paper-based device (μPAD) sensor for the colorimetric detection of glucose based on glucose oxidase/horseradish peroxidase (GOx/HRP) bi-enzymatic system using TMB as chromogenic agent. The μPAD could realize the quantitative detection of glucose within 0.5–2.84 mM, and the detection limit was 0.28 mM. Ultimately, Gabriel et al.[93] documented a colorimetric approach for the quantification of glucose utilizing GOx and HRP enzymes on a paper device, achieving a linear glucose detection range from 0.1 to 1 mM, with a detection limit of 0.05 mM.

Considering that the physiological blood glucose level ranges from 3.0 to 8.0 mM[20]. More specifically, the lower detection limit and significantly extended linearity range observed in this study, comparable to that reported in the literature (Table 2), indicate the great potential of immobilized LDP for glucose detection.

Conclusion

In the current study, recombinant LDP peroxidase was immobilized on a magnetic nanoparticle; the physicochemical properties of LDP-magnetic nanoparticle were investigated, and its potential in glucose detection was examined. Our results demonstrate that covalent immobilization of LDP on nFe_3O_4-CS greatly enhances its functionality, as revealed by higher residual activity and affinity to its substrates. Additionally, thermostability, storage stability, and reusability of the enzyme were improved. The enhanced residual activity and stability of the IE make it suitable for biomedical and food analysis, particularly for glucose detection and reliable quantification. Surprisingly, the glucose detection concentration range increased by more than 10-fold, and the incubation time was reduced by more than 3-fold for the IE compared to the free enzyme.

Further research is needed to increase immobilization efficiency. Further studies using the IE on the other colorimetric biosensors (e.g., cholesterol, urea, etc.) would be more attractive for research. Moreover, the determination of the exact mechanism underlying the improved stability of LDP upon covalent immobilization on chitosan-coated magnetic nanoparticles could provide valuable insights.

Overall, the enhanced reactivity and catalytic efficiency, coupled with enzyme recyclability and strong binding, improved the operational stability of the LDP immobilized on nFe_3O_4-CS-GDA, underscoring the proficiency and effectiveness of the employed support and immobilization methodology. In conclusion, the IE can be introduced as a suitable enzyme for biomolecule detection in clinical practice, enabling precise quantification, and can also be used in various industrial applications.

Data availability

The data from the current study will be made available upon request.

Received: 3 October 2025; Accepted: 22 January 2026
Published online: 03 February 2026

References

1. Bansal, N. & S Kanwar, S. Peroxidase(s) in environment protection. *Sci. World J.* **2013**, 714639. https://doi.org/10.1155/2013/714639 (2013).
2. Cosio, C. & Dunand, C. Specific functions of individual class III peroxidase genes. *J. Exp. Bot.* **60**, 391–408. https://doi.org/10.1093/jxb/ern318 (2009). https://doi.org/https://doi.org/
3. Filiz, B. C., Elalmis, Y. B., Bektaş, İ. S. & Figen, A. K. Fabrication of stable electrospun blended chitosan-poly (vinyl alcohol) nanofibers for designing naked-eye colorimetric glucose biosensor based on GOx/HRP. *Int. J. Biol. Macromol.* **192**, 999–1012 (2021).

4. Ngo, T. T. Peroxidase in chemical and biochemical analysis. *Anal. Lett.* **43**, 1572–1587. https://doi.org/10.1080/00032711003653874 (2010).
5. Weber, A. C. et al. Immobilization of commercial horseradish peroxidase in calcium alginate-starch hybrid support and its application in the biodegradation of phenol red dye. *Int. J. Biol. Macromol.* **246**, 125723 (2023).
6. Liu, C., Tan, L., Zhang, K., Wang, W. & Ma, L. Immobilization of horseradish peroxidase for phenol degradation. *ACS Omega.* **8**, 26906–26915. https://doi.org/10.1021/acsomega.3c01570 (2023). https://doi.org/https://doi/
7. Lopes, G. R., Pinto, D. C. & Silva, A. M. Horseradish peroxidase (HRP) as a tool in green chemistry. *RSC Adv.* **4**, 37244–37265. https://doi.org/10.1039/C4RA06094F (2014).
8. Bonifert, G., Folkes, L., Gmeiner, C., Dachs, G. & Spadiut, O. Recombinant horseradish peroxidase variants for targeted cancer treatment. *Cancer Med.* **5**, 1194–1203. https://doi.org/10.1002/cam4.668 (2016).
9. Altınkaynak, C., Özdemir, N. & Öçsoy, İ. A rational synthesis of magnetic nanoparticles incorporated horseradish peroxidase Nanoflower and its use for the removal of phenol through oxidative coupling reaction with great reusability. *Mugla J. Sci. Technol.* **7**, 59–66. https://doi.org/10.22531/muglajsci.982993 (2021).
10. Vojinovic, V., Cabral, J. M. & Fonseca, L. P. Horseradish peroxidase: A valuable tool in biotechnology. *Biotechnol. Annual Rev.* **9**, 199. https://doi.org/10.1016/S1387-2656(03)09003-3 (2003). https://doi.org/.
11. Chattopadhyay, K. & Mazumdar, S. Structural and conformational stability of horseradish peroxidase: Effect of temperature and pH. *Biochemistry* **39**, 263–270. https://doi.org/10.1021/bi990729o (2000).
12. Veitch, N. C. Horseradish peroxidase: A modern view of a classic enzyme. *Phytochemistry* **65**, 249–259 (2004).
13. Fattahian, Y., Riahi-Madvar, A., Mirzaee, R., Torkzadeh-Mahani, M. & Asadikaram, G. Heterologous expression, purification and characterization of a peroxidase isolated from lepidium Draba. *Protein. J.* **36**, 461–471 (2017).
14. Freitas, C. D. et al. Class III plant peroxidases: From classification to physiological functions. *Int. J. Biol. Macromol.* **263**, 130306 (2024).
15. Kim, E. R., Joe, C., Mitchell, R. J. & Gu, M. B. Biosensors for healthcare: Current and future perspectives. *Trends Biotechnol.* **41**, 374–395. https://doi.org/10.1016/j.tibtech.2022.12.005 (2023).
16. Amine, A., Mohammadi, H., Bourais, I. & Palleschi, G. Enzyme inhibition-based biosensors for food safety and environmental monitoring. *Biosens. Bioelectron.* **21**, 1405–1423. https://doi.org/10.1016/j.bios.2005.07.012 (2006).
17. Nigam, V. K. & Shukla, P. Enzyme based biosensors for detection of environmental pollutants-a review. *J. Microbiol. Biotechnol.* **25**, 1773–1781. https://doi.org/10.4014/jmb.1504.04010 (2015). https://doi.org/http:
18. Alam, F. et al. Lactate biosensing: The emerging point-of-care and personal health monitoring. *Biosens. Bioelectron.* **117**, 818–829. https://doi.org/10.1016/j.bios.2018.06.054 (2018). https://doi.org/https://doi.org/
19. Nemiwal, M., Zhang, T. C. & Kumar, D. Enzyme immobilized nanomaterials as electrochemical biosensors for detection of biomolecules. *Enzym. Microb. Technol.* **156**, 110006. https://doi.org/10.1016/j.enzmictec.2022.110006 (2022).
20. Wen, C. et al. Au@ Cu2O composite nanorods as mimetic peroxidase for glucose colorimetric sensing. *J. Photochem. Photobiol., A.* **455**, 115786. https://doi.org/10.2139/ssrn.4785749 (2024).
21. Zhu, W. J. et al. Bienzyme colorimetric detection of glucose with self-calibration based on tree-shaped paper strip. *Sens. Actuators B.* **190**, 414–418 (2014).
22. Rashtbari, S., Dehghan, G. & Amini, M. An ultrasensitive label-free colorimetric biosensor for the detection of glucose based on glucose oxidase-like activity of nanolayered manganese-calcium oxide. *Anal. Chim. Acta.* **1110**, 98–108. https://doi.org/10.1016/j.aca.2020.03.021 (2020).
23. Zhang, X. et al. Sensitive colorimetric detection of glucose and cholesterol by using Au@ ag core–shell nanoparticles. *RSC Adv.* **6**, 35001–35007. https://doi.org/10.1039/C6RA04976A (2016).
24. Sumitha, M. & Xavier, T. Recent advances in electrochemical biosensors–A brief review. *Hybrid. Adv.* **2**, 100023. https://doi.org/10.1016/j.hybadv.2023.100023 (2023).
25. Gaviria, M. I., Arango, J. P., Barrientos, K. & Jaramillo, M. Optical biosensors for environmental analysis. https://doi.org/10.1016/B978-0-12-822548-6.00156-4 (2023).
26. Nadar, S. S., Vaidya, L. & Rathod, V. K. Enzyme embedded metal organic framework (enzyme–MOF): de Novo approaches for immobilization. *Int. J. Biol. Macromol.* **149**, 861–876 (2020).
27. Keshta, B. E., Gemeay, A. H. & Khamis, A. A. Impacts of horseradish peroxidase immobilization onto functionalized superparamagnetic iron oxide nanoparticles as a biocatalyst for dye degradation. *Environ. Sci. Pollut. Res.* **29**, 6633–6645. https://doi.org/10.1007/s11356-021-16119-z (2022).
28. Maghraby, Y. R., El-Shabasy, R. M., Ibrahim, A. H. & Azzazy, H. M. E.-S. Enzyme immobilization technologies and industrial applications. *ACS Omega.* **8**, 5184–5196. https://doi.org/10.1021/acsomega.2c07560 (2023).
29. Sahu, S., Shera, S. S. & Banik, R. M. Enhanced reusability of horseradish peroxidase immobilized onto graphene oxide/magnetic Chitosan beads for cost effective cholesterol oxidase assay. *Open. Biotechnol. J.* https://doi.org/10.2174/1874070701913010093 (2019).
30. Ahmed, S. A. et al. Catalytic, kinetic and thermal properties of free andimmobilized Bacillus subtilis-MK1 α-amylase on Chitosan-magnetic nanoparticles. *Biotechnol. Rep.* **26**, e00443. https://doi.org/10.1016/j.btre.2020.e00443 (2020).
31. Galvão, W. et al. Novel nanohybrid biocatalyst: Application in the kinetic resolution of secondary alcohols. *J. Mater. Sci.* **53**, 14121–14137 (2018).
32. Choi, M. M. Progress in enzyme-based biosensors using optical transducers. *Microchim. Acta.* **148**, 107–132 (2004).
33. Khoshnevisan, K., Poorakbar, E., Baharifar, H. & Barkhi, M. Recent advances of cellulase immobilization onto magnetic nanoparticles: An update review. *Magnetochemistry* **5**, 36. https://doi.org/10.3390/magnetochemistry5020036 (2019).
34. Zang, L. et al. Preparation of magnetic Chitosan nanoparticles as support for cellulase immobilization. *Ind. Eng. Chem. Res.* **53**, 3448–3454. https://doi.org/10.1021/ie404072s (2014). https://doi.org/http://dx.doi.
35. Mohamed, S. A., Al-Harbi, M. H., Almulaiky, Y. Q., Ibrahim, I. H. & El-Shishtawy, R. M. Immobilization of horseradish peroxidase on Fe3O4 magnetic nanoparticles. *Electron. J. Biotechnol.* **27**, 84–90. https://doi.org/10.1016/j.ejbt.2017.03.010 (2017). https://doi.org/http:
36. Hojnik Podrepšek, G., Knez, Ž. & Leitgeb, M. Development of Chitosan functionalized magnetic nanoparticles with bioactive compounds. *Nanomaterials* **10**, 1913 (2020).
37. Islam, N., Wang, H., Maqbool, F. & Ferro, V. In vitro enzymatic digestibility of glutaraldehyde-crosslinked Chitosan nanoparticles in lysozyme solution and their applicability in pulmonary drug delivery. *Molecules* **24**, 1271. https://doi.org/10.3390/molecules24071271 (2019).
38. Lin, Y. et al. Preparation and characterization of magnetic Fe 3 O 4–chitosan nanoparticles for cellulase immobilization. *Cellulose* **24**, 5541–5550. https://doi.org/10.1007/s10570-017-1520-6 (2017). https://doi.org/.
39. Nouri, M. Green synthesis of Chitosan magnetic nanoparticles and their application with poly-aldehyde Kefiran cross-linker to immobilize pectinase enzyme. *Biocatal. Agric. Biotechnol.* **29**, 101681. https://doi.org/10.1016/j.bcab.2020.101681 (2020).
40. Petrucci, R., Pasquali, M., Scaramuzzo, F. A. & Curulli, A. Recent advances in electrochemical chitosan-based chemosensors and biosensors: Applications in food safety. *Chemosensors* **9**, 254. https://doi.org/10.3390/chemosensors9090254 (2021).
41. Ananias Reis, D. et al. Electrochemical biosensor based on Gherkin (Cucumis anguria) peroxidase immobilized on chitosan-coated iron oxide nanoparticles for phenolic compounds detection. *Electroanalysis* **37**, 202400251 (2025). https://doi.org/10.1002/elan.202400251

42. Devi, R. & Pundir, C. Construction and application of an amperometric uric acid biosensor based on covalent immobilization of uricase on iron oxide nanoparticles/chitosan-g-polyaniline composite film electrodeposited on Pt electrode. *Sens. Actuators B.* **193**, 608–615. https://doi.org/10.1016/j.snb.2013.12.010 (2014).
43. Fatoni, A., Hidayah, V. F., Suyata, S., Diastuti, H. & Anggraeni, M. D. Chitosan–Fe3O4 nanoparticles cryogel for glucose biosensor development. *Sci. Technol. Indonesia*. **8**, 52–58. https://doi.org/10.26554/sti.2023.8.1.52-58 (2023).
44. Luo, L. et al. Hydrogen peroxide biosensor based on horseradish peroxidase immobilized on chitosan-wrapped NiFe 2 O 4 nanoparticles. *Microchim. Acta*. **174**, 55–61. https://doi.org/10.1007/s10008-010-1120-y (2011).
45. K Laemmli, U. Cleavage of structural proteins during the assembly of the head of bacteriophage T4. *Nature* **227**, 680–685. https://doi.org/10.1038/227680a0 (1970).
46. Bradford, M. M. A rapid and sensitive method for the quantitation of microgram quantities of protein utilizing the principle of protein-dye binding. *Anal. Biochem.* **72**, 248–254. https://doi.org/10.1016/0003-2697(76)90527-3 (1976).
47. Krainer, F. W. et al. Purification and basic biochemical characterization of 19 Recombinant plant peroxidase isoenzymes produced in Pichia pastoris. *Protein Exp. Purif.* **95**, 104–112. https://doi.org/10.1016/j.pep.2013.12.003 (2014). https://doi.org/https://doi.org/
48. Lin, Y. et al. Preparation and characterization of magnetic Fe3O4–chitosan nanoparticles for cellulase immobilization. *Cellulose* **24**, 5541–5550. https://doi.org/10.1007/s10570-017-1520-6 (2017). https://doi.org/https://link.springer.com/article/
49. Wang, L. L., Fan, M., Xing, X., Liu, Y. & Sun, S. Immobilization of glyceraldehyde-3-phosphate dehydrogenase on Fe3O4 magnetic nanoparticles and its application in Histamine removal. *Colloids Surf., B.* **205**, 111917. https://doi.org/10.1016/j.colsurfb.2021.111917 (2021).
50. Abdella, M. A., Ahmed, S. A. & Hassan, M. E. Protease immobilization on a novel activated carrier alginate/dextrose beads: Improved stability and catalytic activity via covalent binding. *Int. J. Biol. Macromol.* **230**, 123139. https://doi.org/10.1016/j.ijbiomac.2023.123139 (2023).
51. El-Shishtawy, R. M., Ahmed, N. S. & Almulaiky, Y. Q. Immobilization of catalase on chitosan/ZnO and chitosan/ZnO/Fe2O3 nanocomposites: A comparative study. *Catalysts* **11**, 820 (2021).
52. Jin, S., Liu, L., Fan, M., Jia, Y. & Zhou, P. A facile strategy for immobilizing GOD and HRP onto pollen grain and its application to visual detection of glucose. *Int. J. Mol. Sci.* **21**, 9529 (2020).
53. Nouaa, S., Aziam, R., Carja, G., Chiban, M. & Froidevaux, R. Immobilization of trametes versicolor laccase on LDH/alginate composite beads for improved textile dyes decolorization. *Int. J. Biol. Macromol.* **303**, 140577 (2025).
54. Chang, Q. & Tang, H. Immobilization of horseradish peroxidase on NH2-modified magnetic Fe3O4/SiO2 particles and its application in removal of 2, 4-dichlorophenol. *Molecules* **19**, 15768–15782. https://doi.org/10.3390/molecules191015768 (2014).
55. Lu, Y. M. et al. Enhanced activity of immobilized horseradish peroxidase by carbon nanospheres for phenols removal. *CLEAN–Soil Air Water*. **45**, 1600077. https://doi.org/10.1002/clen.201600077 (2017).
56. Zhai, R. et al. Chitosan–halloysite hybrid-nanotubes: Horseradish peroxidase immobilization and applications in phenol removal. *Chem. Eng. J.* **214**, 304–309. https://doi.org/10.1016/j.cej.2012.10.073 (2013). https://doi.org/https://doi.org/
57. Jankowska, K., Sigurdardóttir, S. B., Zdarta, J. & Pinelo, M. Co-immobilization and compartmentalization of cholesterol oxidase, glucose oxidase and horseradish peroxidase for improved thermal and H2O2 stability. *J. Membr. Sci.* **662**, 121007 (2022).
58. Gomez, J. et al. Immobilization of peroxidases on glass beads: An improved alternative for phenol removal. *Enzym. Microb. Technol.* **39**, 1016–1022 (2006).
59. Chagas, P. M. B. et al. Catalytic stability of turnip peroxidase in free and immobilized form on Chitosan beads. *Int. J. Curr. Microbiol. Appl. Sci.* **3**, 576–595 (2014).
60. Díaz-Hernández, A. et al. Characterization of magnetic nanoparticles coated with chitosan: A potential approach for enzyme immobilization. *J. Nanomater.* **2018**, 9468574 (2018).
61. Monier, M., Ayad, D., Wei, Y. & Sarhan, A. Immobilization of horseradish peroxidase on modified chitosan beads. *Int. J. Biol. Macromol.* **46**, 324–330. https://doi.org/10.1016/j.ijbiomac.2009.12.018 (2010).
62. Hosseini, F., Sadighian, S., Hosseini-Monfared, H. & Mahmoodi, N. M. Dye removal and kinetics of adsorption by magnetic chitosan nanoparticles. *Desalination Water Treat.* **57**, 24378–24386. https://doi.org/10.1080/19443994.2016.1143879 (2016).
63. Usoltsev, D., Sitnikova, V., Kajava, A. & Uspenskaya, M. FTIR spectroscopy study of the secondary structure changes in human serum albumin and trypsin under neutral salts. *Biomolecules* **10**, 606. https://doi.org/10.3390/biom10040606 (2020).
64. Singh, A. N., Singh, S., Suthar, N. & Dubey, V. K. Glutaraldehyde-activated Chitosan matrix for immobilization of a novel cysteine protease, Procerain B. *J. Agric. Food Chem.* **59**, 6256–6262. https://doi.org/10.1021/jf200472x (2011).
65. Patel, S. K., Choi, S. H., Kang, Y. C. & Lee, J. K. Eco-friendly composite of Fe3O4-reduced graphene oxide particles for efficient enzyme immobilization. *ACS Appl. Mater. Interfaces*. **9**, 2213–2222. https://doi.org/10.1021/acsami.6b05165 (2017). https://doi.org/http:
66. Chang, Q. et al. Enzymatic removal of Chlorophenols using horseradish peroxidase immobilized on superparamagnetic Fe3O4/graphene oxide nanocomposite. *Chin. J. Catal.* **36**, 961–968. https://doi.org/10.1016/S1872-2067(15)60856-7 (2015). https://doi.org/.
67. Muley, A. B., Mulchandani, K. H. & Singhal, R. S. in *Methods in enzymology* Vol. 630 39–79 (Elsevier, 2020).
68. Bangoria, P., Chaki, S. & Shah, A. R. Immobilization of fungal α-galactosidase on magnetic nanoparticles and hydrolysis of raffinose family oligosaccharides (RFO) in soymilk. *Biocatal. Biotransform.* **42**, 388–400. https://doi.org/10.1080/10242422.2023.2247516 (2024).
69. Kalsoom, U. et al. Biocatalytic degradation of reactive blue 221 and direct blue 297 dyes by horseradish peroxidase immobilized on iron oxide nanoparticles with improved kinetic and thermodynamic characteristics. *Chemosphere* **312**, 137095. https://doi.org/10.1016/j.chemosphere.2022.137095 (2023).
70. Farhadi, S., Riahi-Madvar, A., Sargazi, G. & Mortazavi, M. Immobilization of lepidium Draba peroxidase on a novel Zn-MOF nanostructure. *Int. J. Biol. Macromol.* **173**, 366–378. https://doi.org/10.1016/j.ijbiomac.2020.12.216 (2021).
71. Jonović, M. et al. Immobilization of horseradish peroxidase on magnetite-alginate beads to enable effective strong binding and enzyme recycling during anthraquinone dyes' degradation. *Polymers* **14**, 2614. https://doi.org/10.3390/polym14132614 (2022).
72. Fang, H., Huang, J., Ding, L., Li, M. & Chen, Z. Preparation of magnetic Chitosan nanoparticles and immobilization of laccase. *J. Wuhan Univ. Technology-Mater Sci. Ed.* **24**, 42–47. https://doi.org/10.1007/s11595-009-1042-7 (2009). https://doi.org/http:
73. Xie, X. et al. Horseradish peroxidase immobilized on the magnetic composite microspheres for high catalytic ability and operational stability. *Enzym. Microb. Technol.* **122**, 26–35. https://doi.org/10.1016/j.enzmictec.2018.12.007 (2019). https://doi.org/https://doi.
74. Silveira, T. R. et al. An efficient decolorization of Methyl orange dye by laccase from Marasmiellus palmivorus immobilized on chitosan-coated magnetic particles. *Biocatal. Agric. Biotechnol.* **30**, 101859 (2020).
75. Riahi-Madvar, A., Mortazavi, M. & Torkzadeh-Mahani, M. Effect of Arg186 and Arg198 substitutions on the catalytic, structural, and stability properties of the peroxidase from lepidium Draba. *Int. J. Biol. Macromol.* https://doi.org/10.1016/j.ijbiomac.2025.146802 (2025).
76. Huang, S. H., Liao, M. H. & Chen, D. H. Direct binding and characterization of lipase onto magnetic nanoparticles. *Biotechnol. Prog.* **19**, 1095–1100. https://doi.org/10.1021/bp025587v (2003).
77. Abdel-Hameed, S. A., Ahmed, S. A., Mostafa, F. A., Almasarawi, O. N. & Wahab, W. A. A. Preparation and characterization of Sugilite glass from basalt for α-amylase immobilization, statistical optimization of the immobilization process and description of free and immobilized enzyme. *Heliyon* https://doi.org/10.1016/j.heliyon.2022.e09960 (2022).

78. Siddeeg, S. M., Tahoon, M. A., Mnif, W. & Ben Rebah, F. Iron oxide/chitosan magnetic nanocomposite immobilized manganese peroxidase for decolorization of textile wastewater. *Processes* **8**, 5. https://doi.org/10.3390/pr8010005 (2019).
79. Aydemir, T. & Güler, S. Characterization and immobilization of trametes versicolor laccase on magnetic chitosan–clay composite beads for phenol removal. *Artif. Cells Nanomed. Biotechnol.* **43**, 425–432 (2015).
80. Gao, X. et al. Immobilization of horseradish peroxidase on hierarchically porous magnetic metal-organic frameworks for visual detection and efficient degradation of 2, 4-dichlorophenol in simulated wastewater. *Biochem. Eng. J.* **190**, 108760 (2023).
81. Amaro-Reyes, A. et al. Enhanced performance of immobilized xylanase/filter paper-ase on a magnetic Chitosan support. *Catalysts* **9**, 966. https://doi.org/10.3390/catal9110966 (2019).
82. Jaiswal, N., Pandey, V. P. & Dwivedi, U. N. Immobilization of Papaya laccase in Chitosan led to improved multipronged stability and dye discoloration. *Int. J. Biol. Macromol.* **86**, 288–295. https://doi.org/10.1016/j.ijbiomac.2016.01.079 (2016).
83. Vineh, M. B., Saboury, A. A., Poostchi, A. A., Rashidi, A. M. & Parivar, K. Stability and activity improvement of horseradish peroxidase by covalent immobilization on functionalized reduced graphene oxide and biodegradation of high phenol concentration. *Int. J. Biol. Macromol.* **106**, 1314–1322 (2018).
84. Ibrahim, A. S. S. et al. Enhancement of alkaline protease activity and stability via covalent immobilization onto Hollow core-mesoporous shell silica nanospheres. *Int. J. Mol. Sci.* **17**, 184. https://doi.org/10.3390/ijms17020184 (2016).
85. Wang, X. Y., Jiang, X. P., Li, Y., Zeng, S. & Zhang, Y. W. Preparation Fe3O4@ Chitosan magnetic particles for covalent immobilization of lipase from thermomyces lanuginosus. *Int. J. Biol. Macromol.* **75**, 44–50. https://doi.org/10.1016/j.ijbiomac.2015.01.020 (2015).
86. Habimana, P. et al. Improvement of laccase activity via covalent immobilization over mesoporous silica coated magnetic multiwalled carbon nanotubes for the discoloration of synthetic dyes. *ACS Omega*. **6**, 2777–2789. https://doi.org/10.1021/acsomega.0c05081 (2021).
87. Mohammadi, M. et al. Immobilization of laccase on epoxy-functionalized silica and its application in biodegradation of phenolic compounds. *Int. J. Biol. Macromol.* **109**, 443–447. https://doi.org/10.1016/j.ijbiomac.2017.12.102 (2018). https://doi.org/http://dx.doi.
88. Kaushal, J., Singh, G. & Arya, S. K. Immobilization of catalase onto chitosan and chitosan–bentonite complex: A comparative study. *Biotechnol. Rep.* **18**, e00258 (2018). https://doi.org/10.1016/j.btre.2018.e00258
89. Long, Y., Pan, Y., Zheng, W., Yi, D. & Zheng, H. Supramolecular hydrogel-immobilized enzyme Ficin as peroxidase mimics for colorimetric detection of glucose. *Microchem. J.* **158**, 105276. https://doi.org/10.1016/j.microc.2020.105276 (2020).
90. Skonta, A., Bellou, M. G., Matikas, T. E. & Stamatis, H. Colorimetric glucose biosensor based on Chitosan films and its application for glucose detection in beverages using a smartphone application. *Biosensors* **14**, 299 (2024).
91. Soni, A. & Jha, S. K. A paper strip based non-invasive glucose biosensor for salivary analysis. *Biosens. Bioelectron.* **67**, 763–768 (2015).
92. Zhang, H. et al. A low-cost mobile platform for whole blood glucose monitoring using colorimetric method. *Microchem. J.* **162**, 105814 (2021).
93. Gabriel, E. F. M., Garcia, P. T., Lopes, F. M. & Coltro, W. K. T. Based colorimetric biosensor for tear glucose measurements. *Micromachines* **8**, 104 (2017).

Author contributions

Author Contributions Statement Mohadeseh Sepahi-Baghan: Investigation, Software, Writing- Original draft preparation; A. Asoodeh: Funding, Supervision, Validation, Writing- Reviewing and Editing; Ali Riahi-Madvar: Supervision, Validation, Writing- Reviewing and Editing.

Funding

The authors appreciate the support provided by the Research and Technology Council of the Ferdowsi University of Mashhad, Iran (grant numbers: 3/59600 and 1402/01/22).

Declarations

Competing interests

The authors declare no competing interests.

Additional information

Correspondence and requests for materials should be addressed to A.A. or A.R.-M.